# Frequency-Wavenumber Spectra of Sea Surface Temperature and Wind-Stress Curl in the Eastern North Pacific

ARTEMIO GALLEGOS-GARCIA

*Centro de Ciencias del Mar y Limnologia, Universidad Nacional Autónoma de México, México 20*

WILLIAM J. EMERY

*Department of Oceanography, University of British Columbia, Vancouver, B.C., Canada V6T 1W5*

ROBERT O. REID

*Department of Oceanography, Texas A & M University, College Station 77843*

LORENZ MAGAARD

*Department of Oceanography, University of Hawaii, Honolulu 96832*

(Manuscript received 6 January 1981, in final form 20 April 1981)

ABSTRACT

Frequency-wavenumber spectra of sea surface temperature and wind-stress curl are computed from 11 years of surface marine observations taken in the eastern North Pacific. These data were averaged by month and 2° quadrangles to yield spectra with periods from 2 to 48 months and zonal wavelengths from 400 to 4000 km. Spectra were computed for all 2° zonal bands between 16 and 40°N using data from the area between 120 and 160°W. Missing monthly values led to the computation of these spectra using a least-squares Fourier expansion which eliminated the need for temporal interpolation. Frequency spectra computed with this technique compare well with spectra using standard Fourier methods.

The resulting spectra were found to separate naturally into two regions; one between 29 and 40°N and the second between 15 and 29°N. Even within these zonal bands there were some important north–south changes. The annual signal was found to dominate the spectra of sea surface temperature at almost all wavelengths. The semiannual and 2-year periods were often also significant in sea surface temperature spectra. The annual peak dominated many of the wind-stress curl spectra at the longest wavelengths (~2000–4000 km). Most of the energetic peaks in all spectra were symmetric with respect to east–west wavenumber. There were, however, some asymmetries suggesting both east and westward phase propagation. Generally, wind-stress curl spectra were white in frequency and red in wavenumber while sea surface temperature spectra were red in wavenumber but dominated by the 2-year, annual and semiannual periods in frequency.

## 1. Introduction

The generation of low-frequency oceanic motions by atmospheric forcing has become a topic of current research. In a recent study Willebrand *et al.* (1980) discuss the forced barotropic response of a linear ocean model using a frequency-wavenumber spectrum of wind-stress curl as the forcing. They found that at forcing periods between the inertial and one week there is little or no coherence between the input and response spectra. For periods of a week to a month planetary Rossby waves dominate the response. At longer forcing periods they found that the ocean settles down to a Sverdrup-type balance between meridional currents and wind-stress curl. As a guide to the idealized wind-stress curl spectrum they referred to an earlier study (Willebrand, 1978) which used synoptic sea level pressure maps to produce spectra of wind stress and wind-stress curl. The spectral window in these calculations stretched from days to months and from 1000 km to the size of the ocean basin. The characteristics of the resulting input wind-stress curl spectrum were 1) white in frequency at periods longer than a few days and 2) red in wavenumber.

Similar theoretical input spectra were employed by Frankignoul and Müller (1979a) in their discussion of the stochastic forcing of mesoscale eddies. This spectral character had been selected after the examination of available spectra of wind and wind-stress curl (Kao, 1970; Wilson, 1975). Frankignoul and Müller (1979a) conclude that wind stress curl (WSCL) fluctuations could be an important generating source for mesoscale eddies. In a later paper

0022-3670/81/081059-19$08.75

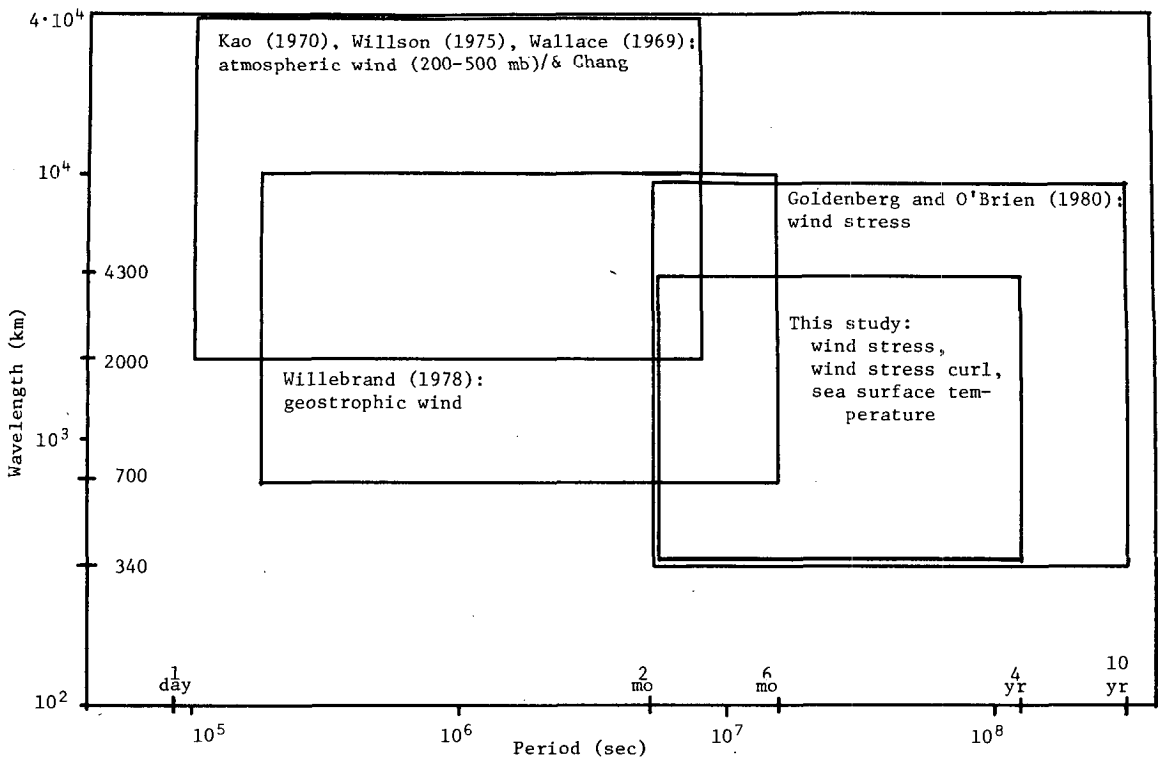


FIG. 1. Space-time scales in spectral studies of atmospheric forcing.

(Frankignoul and Müller, 1979b) an analogous theoretical description of a sea surface temperature (SST) frequency-wavenumber spectrum is used to estimate the quasi-geostrophic oceanic response to changes in buoyancy flux. This input spectrum has an annual peak in frequency and decreases with the square of frequency. It also has a $-2$ slope with increasing zonal wavenumber. They report that these buoyancy flux variations are not likely to generate quasi-geostrophic motions.

In an earlier theoretical study, Magaard (1977) suggested that both buoyancy flux (represented by SST) and WSCL fluctuations could be strong enough to force a subinertial response in the ocean. Motivated by observations of Rossby waves in the eastern North Pacific (Emery and Magaard, 1976), the present study calculates frequency-wavenumber spectra of WSCL and SST as possible input to models similar to that of Magaard (1977).

The data utilized in these spectral computations came from the ship weather observations collectively referred to as the Surface Marine Deck. Although the wind measurements represent a wide range of accuracy and reliability they are, at present, the only source of wind data over the open ocean. Thus unless we wish to wait until years (11 years of monthly averages are used in this study) of reliable wind data from satellites are available, we must work carefully with the Marine Deck observations to gain some insight into the frequency-wavenumber character of WSCL over the ocean.

Recent studies (Wyrtki and Meyers, 1976) of Surface Marine Deck wind data from the equatorial Pacific (30°N to 30°S) have found these data to be very coherent in the form of monthly averaged vector fields. Using a subjective technique to fill in data gaps. Goldenberg and O'Brien (1981) use these same equatorial Pacific wind data to compute frequency-wavenumber spectra.

The present study restricts its region of interest to the area from 10 to 40°N, 120 to 160°W in the North Pacific. In frequency-wavenumber scale it overlaps with the study by Goldenberg and O'Brien (1981) as shown in Fig. 1. Other data studies of WSCL spectra, discussed above, cover very different scales as shown in this diagram. It should be mentioned that in contrast to the equatorial analysis of Goldenberg and O'Brien no subjective interpolation was used in the present work.

This paper further describes the data used in the study and discusses the least-squares Fourier transform technique used to calculate the frequency-wavenumber spectra from sometimes gappy time series. These two-dimensional frequency-wavenumber spectra are presented for individual 2° zonal bands as well as for areal averages for the tropical (16–29°N) and subtropical (29–40°N) bands. In addition, one-dimensional composite spectra (re-

duced by averaging to either frequency or zonal wavenumber spectra) are presented for these two average bands. These spectra are compared with the present concepts of such forcing spectra and their utility as input for oceanic response models is discussed.

## 2. Data

All of the data analyzed in this study came from the Surface Marine Deck of the Environmental Data Service in Asheville, North Carolina. Wind speed observations were originally recorded in the Beaufort scale and were converted to wind speed ($m\ s^{-1}$) using the World Meteorological Organization's code 1100 (Wyrtki and Meyers, 1976). Wind direction also was estimated by the observers. Maps of the mean wind fields from these data compare very well with the overlapping region described by Wyrtki and Meyers.

Ship injection temperatures taken from thermometers mounted in the seawater intake of the engine cooling system were used for SST observations. These injection temperatures have been reported (Saur, 1963; Kenyon, 1977; Tabata, 1978) to show an offset when compared to simultaneous surface bucket temperatures. In the present study only the fluctuations of SST are considered. Hence the bias of the injection temperatures should not influence the results.

The number of both wind and SST observations by 2° quadrangles (Fig. 2) limits the region of investigation to latitudes from 16 to 40°N and longitudes from 120 to 160°W. The best temporal coverage in terms of monthly averages was between January 1960 and December 1971. Over this period a total of 675 460 SST measurements and 695 691 wind observations were available for study. These data were originally averaged and sorted by 1° squares but the paucity of data, especially at the lower latitudes, necessitated the added averaging over 2° quadrangles. Of the resulting 240 2° squares ~ 70% have at least 20 observations per month. Nevertheless, 36% of the time series in the 2° quadrangles had no observations for some months. Fortunately, the number of missing data

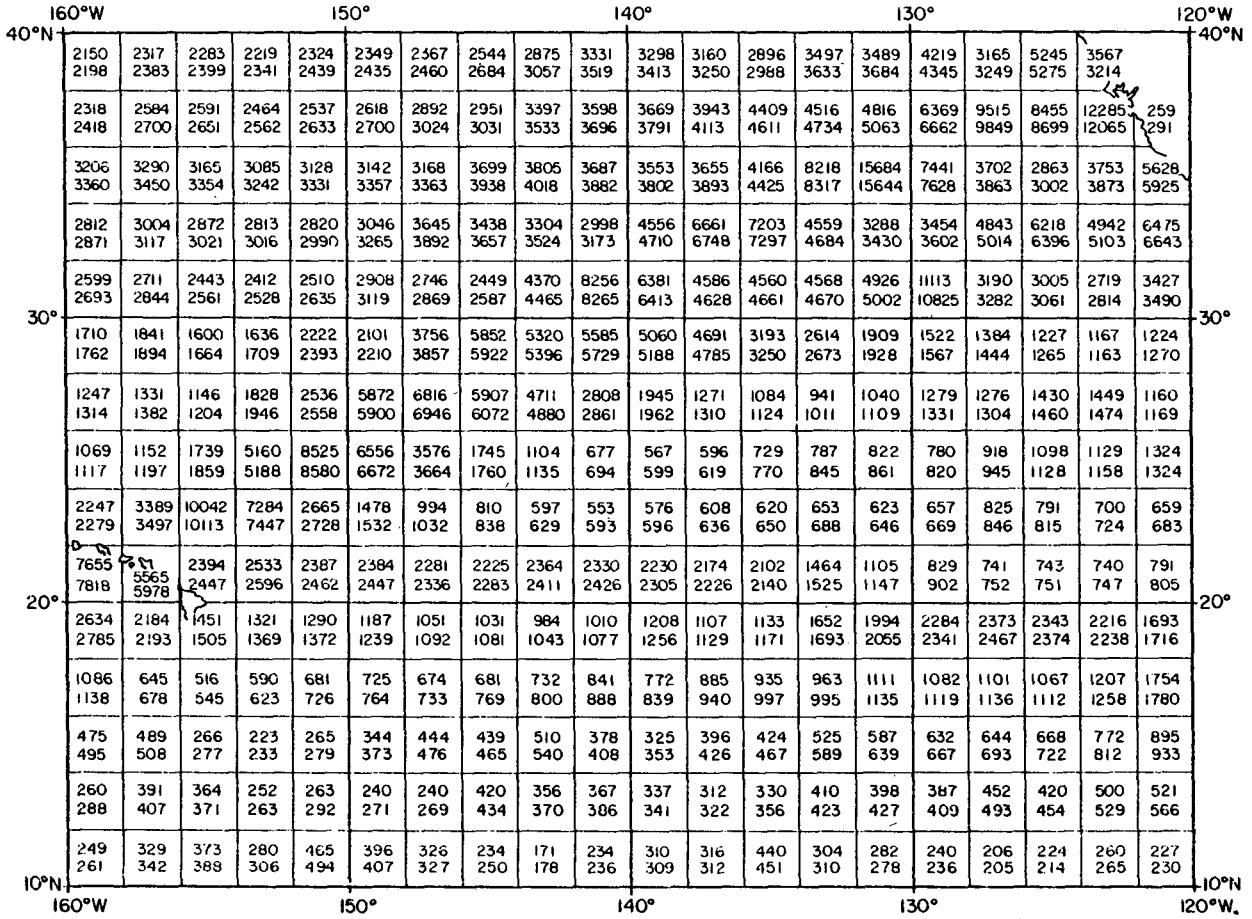


FIG. 2. The number of observations of wind (lower) and sea surface temperature (upper) by 2° squares for the period between 1961 and 1972.

was not large with only 3% of all the series having up to 25 missing points out of a 132-point time series. In the original 1° square averaging data points lying outside of ±2 standard deviations were rejected.

From the monthly averages of zonal ($u$) and meridional ($v$) wind, corresponding wind-stress components were computed as

$$[\tau_x, \tau_y] = \rho_a C_D[u, v]|\bar{V}|, \quad (1)$$

where $\tau_x$ and $\tau_y$ are the zonal and meridional wind stresses, $\rho_a$ the air density, $C_D$ the constant drag coefficient ($1.5 \times 10^{-3}$) and $|\bar{V}|$ the magnitude of the wind vector. Both the wind and wind-stress components were assumed to apply to the center of the 2° square over which the data were averaged.

The curl of the wind stress (WSCL) was computed, using finite-difference techniques, from the 2° square wind-stress values. The zonal derivative was scaled by the cosine of the mean latitude to make the WSCL independent of latitude. The resulting time series of WSCL were then assigned to the border intersection between four adjacent 2° quadrangles. This somewhat reduced the total number of series considered and restricted the maximum wavelength slightly. Maps of WSCL from these data only generally resemble similar maps in Willebrand (1978) and Wyrtki and Meyers (1976). Discrepancies may be due to the very much smaller grid spacing used in this study (Saunders, 1976).

## 3. Spectral method

The computation of the frequency-wavenumber spectra was accomplished by a twice repeated application of the Fourier transform. The first application, applied to time, yielded the Fourier coefficients to describe the data in frequency. These coefficients were then transformed to give a final four coefficients (see the Appendix) which, when appropriately combined, comprise the complete frequency-wavenumber variance spectrum (as distinguished from spectral density).

The presence of missing monthly values in the initial time series, for many of the 2° squares, prohibited the application of standard Fourier frequency transform techniques. It was decided that rather than employ some interpolation technique (linear or otherwise), to fill these data gaps, we would use a least-squares Fourier expansion (LSFT) to fit the available data points (see the Appendix). In this way less than a complete Fourier set was required and missing time series values could be tolerated. Using this technique has the effect of filling in the gaps from information on the entire time series record.

Through the use of the LSFT all the 2° squares had coefficients for the frequency transform. Thus traditional Fourier methods were employed to calculate the spatial Fourier transform. Since the number of total values was relatively few (~200) a direct Fourier transform was used rather than the more popular fast Fourier transform. The resulting coefficients were properly combined (see the Appendix) and plotted for the appropriate regions of frequency and positive (eastward)/negative (westward) wavenumber.

All time series utilized in this study were 11-year records of monthly means. To increase the statistical reliability of the spectra the fundamental period was chosen as 4 years (48 months). Thus the frequency axis runs from 1/48 to ½ cycles per month (cy mon$^{-1}$). The 2° square averaging resulted in a spatial grid size of ~220 km. The longitude range selected was from 120 to 160°W giving a wavenumber scale from 1/20 to ½ cycles per 2° square corresponding to wavenumbers between 0.23 and 2.3 cycles per 1000 km [cy (1000 km)$^{-1}$]. Thus periods range from two months to four years and wavenumbers range approximately from 400 to 4000 km. We will refer to the largest values as long wavelengths and periods while those near the Nyquist values will be called short. The units for all frequency-wavenumber variance spectra are in terms of the square of the variable in question. For example, the spectral values in the SST spectra have units of °C$^2$.

It was difficult to estimate the appropriate degrees of freedom in the LSFT method used. Comparison between the LSFT and other standard Fourier methods (Appendix) suggested that for the present application each spectral estimate should have at least six degrees of freedom for the initial frequency transform. Therefore the subsequent transform (to produce the frequency-wavenumber spectra) should have 12 degrees of freedom for each spectral value. The confidence intervals for all two-dimensional (frequency-wavenumber) spectra were computed using 12 degrees of freedom.

Since a uniform confidence interval can be used for log spectra, the frequency-wavenumber spectra presented are plotted as $\log_2(E_z)$, where $E_z$ is a spectral value. A base 2 rather than a base 10 system was used in the output scale. At the 90% level the confidence interval stretches over two contour intervals in the $\log_2$ system. Thus any values, separated by at least two contours, are significantly different at the 90% level.

In an effort to present the spectra in a more familiar way composite spectra were computed by averaging over either frequency or wavenumber. Thus a two-dimensional variance spectrum was reduced to either a frequency spectrum (averaging over wavenumber) or a wavenumber spectrum (averaging over frequency). All of these one-dimensional spectra were then converted to spectral

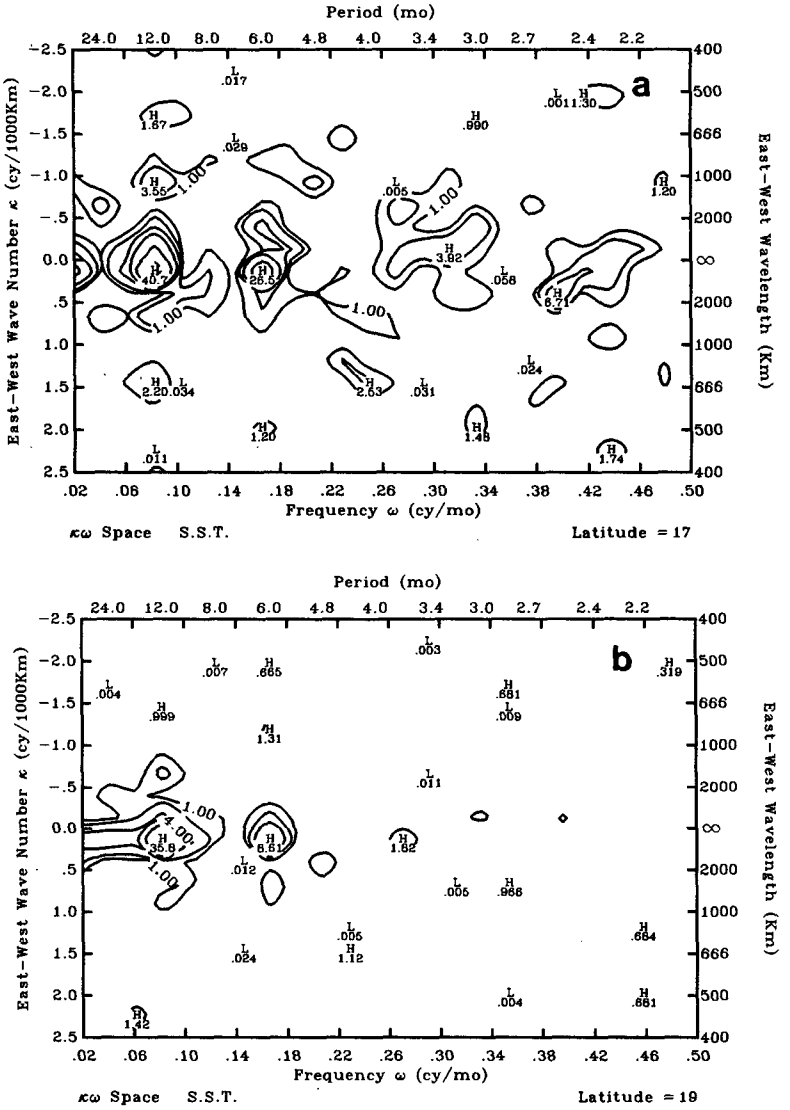


FIG. 3. Frequency-wavenumber spectra of sea surface temperature ($\log_2$ °C$^2$) for the 2° zonal band centered at around (a) 17°N, (b) 19°N, (c) 21°N, (d) 23°N, (e) 25°N, (f) 27°N, (g) 29°N, (h) 31°N, (i) 33°N, (j) 35°N, (k) 37°N and (l) 39°N.

density spectra by dividing the spectral values by either the frequency interval (frequency spectra) or the wavenumber interval (wavenumber spectra).

The statistical reliability of these composite spectra increases over the two-dimensional spectra due to the averaging. If all the series averaged were independent the total degrees of freedom per spectral value would be 288 for the composite frequency spectra and 240 for the composite wavenumber spectra. Thus the correct degrees of freedom must lie between these maxima and the input value of 12. Without any practical, and computationally inexpensive method to compute the degrees of freedom for the composite spectra, it was assumed that approximately one of every six spectral points was independent. Hence each one-dimensional spectral estimate had about 50 degrees of freedom. The corresponding 90% confidence intervals are displayed for each of the composite spectra.

## 4. Frequency-wavenumber spectra

### *a. Sea surface temperature*

The frequency-zonal wavenumber spectra of SST are presented in Figs. 3a–3l. Each panel corresponds to a 2° zonal band centered on the latitude given. Going from south to north these spectra reveal some interesting and significant meridional changes. The annual period dominates the low

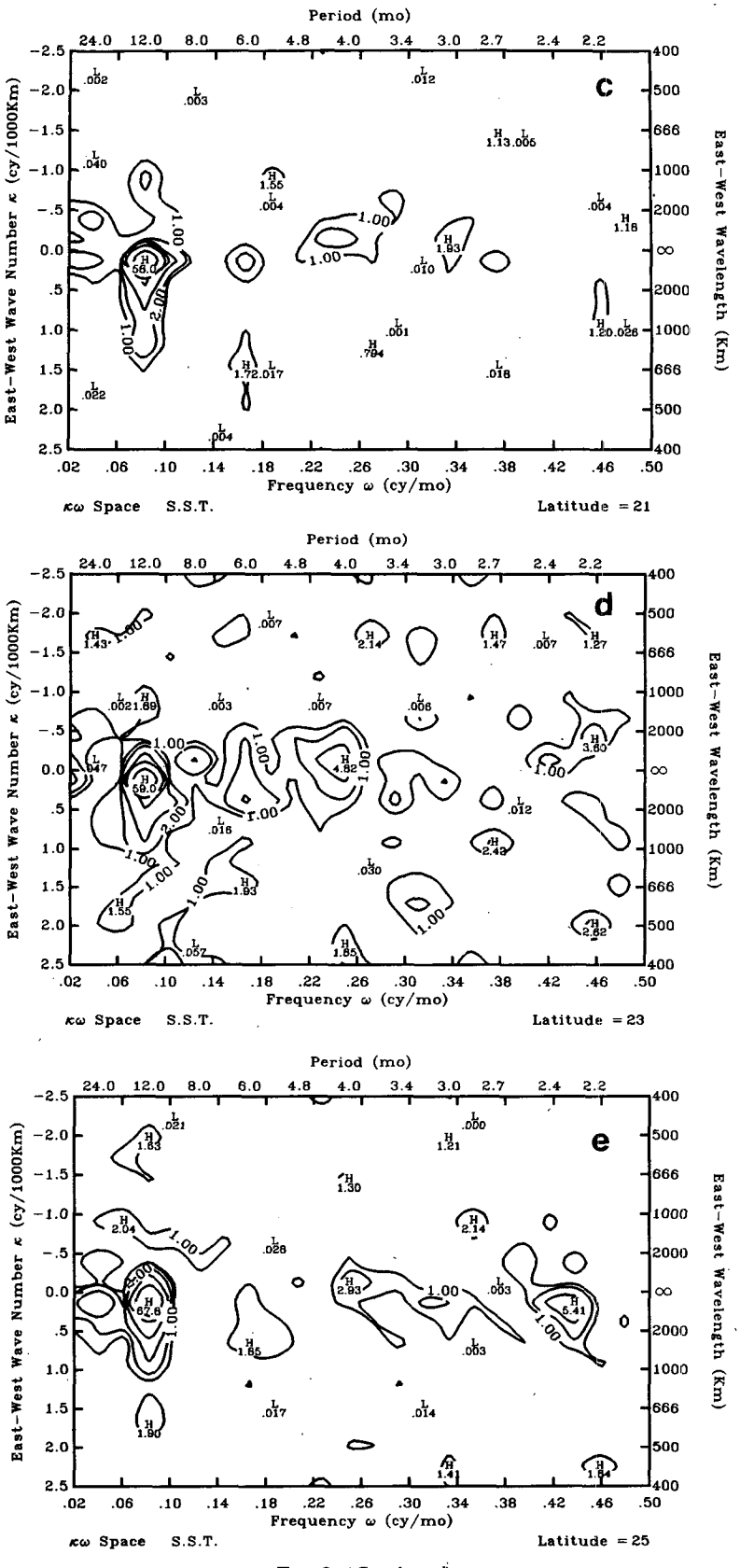


FIG. 3. (*Continued*)

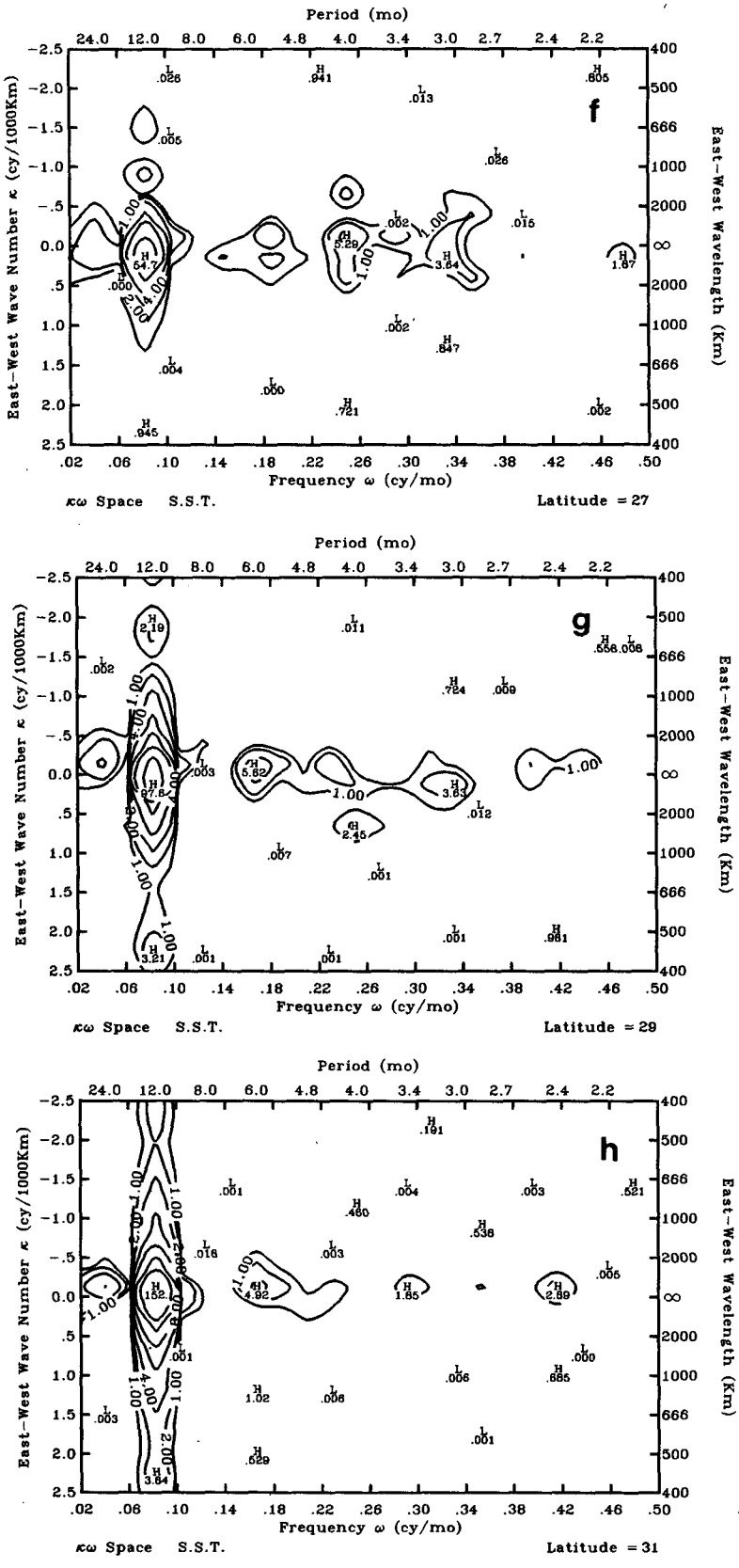


FIG. 3. (*Continued*)

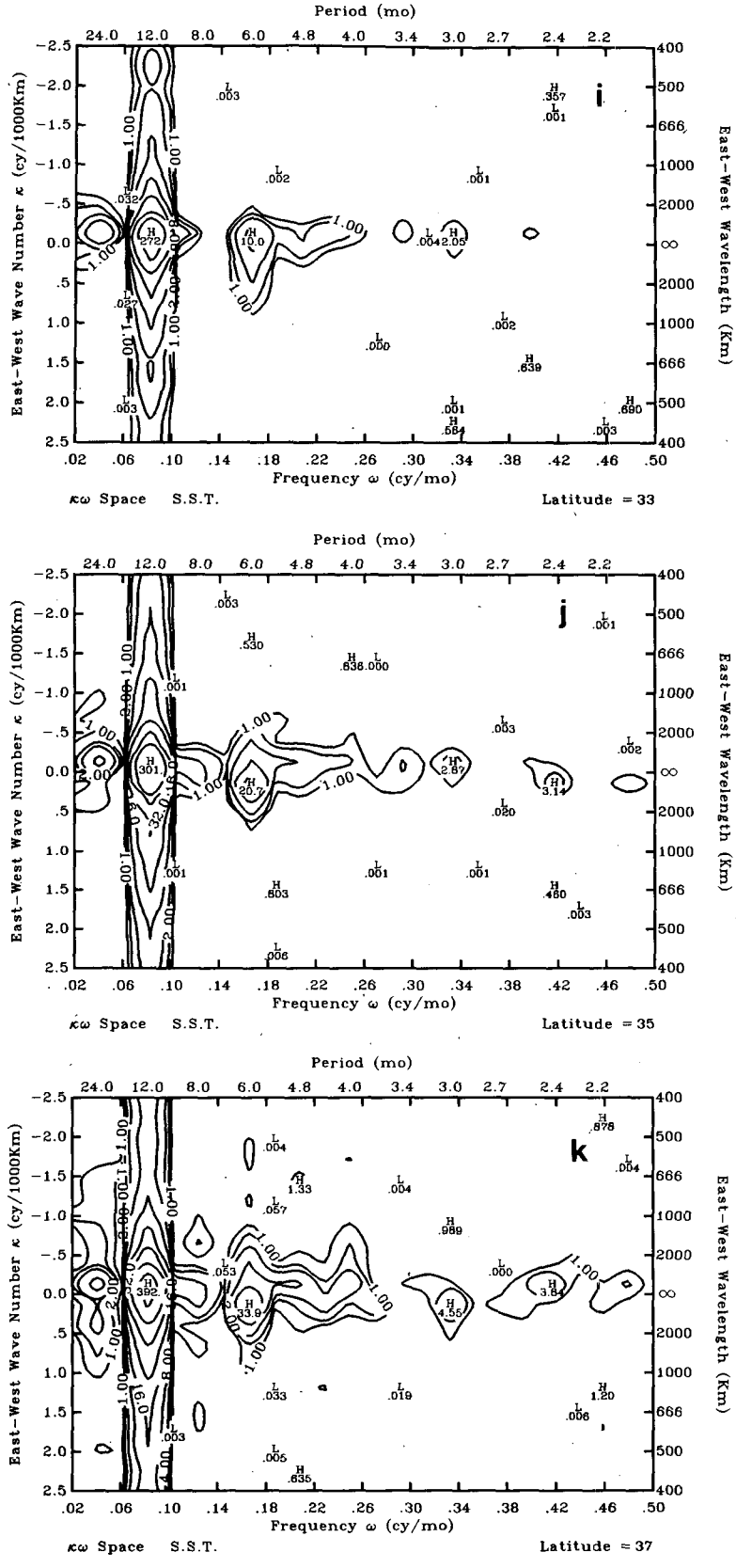


FIG. 3. (*Continued*)

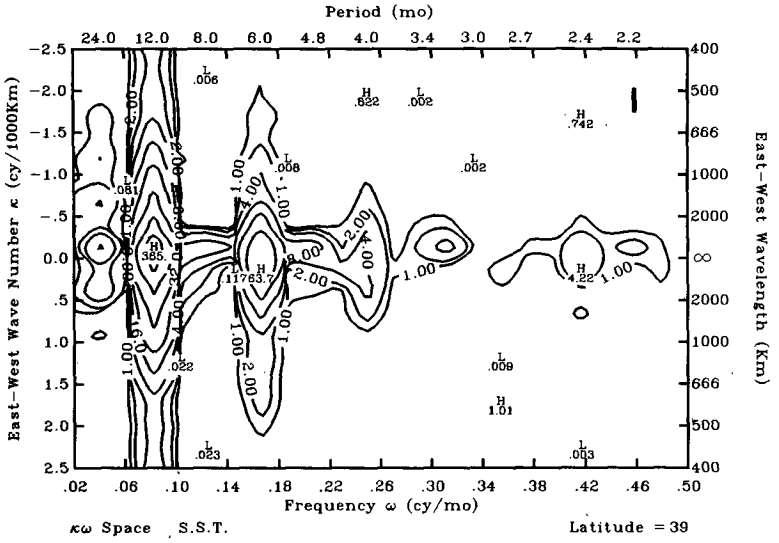


FIG. 3. (*Continued*)

wavenumbers for all zonal bands and becomes increasingly important for higher wavenumbers in spectra farther north. This annual peak appears symmetric with wavenumber in all but the bands between 21 and 25°N (Figs. 3c–3e) where there is some suggestion of eastward asymmetry. No effort was made to eliminate the annual peak and study only the anomaly spectral patterns. An analysis of the possible spectral leakage of the annual signal into higher harmonics revealed that only 30% of the semiannual (6-month) peak could be explained by this contamination.

Next to the annual peak the semiannual (6-month) peak exhibits the greatest spectral energy in most bands. As with the annual period the 6-month peak is limited to the longest wavelengths in the southern bands and extends to shorter wavelengths at higher latitudes. In these northern spectra there is some suggestion of eastward asymmetry in the semiannual peak (Figs. 3i and 3j).

Between latitudes 21 and 27°N (Figs. 3c–3f) the 6-month peak disappears yielding the role of secondary maximum to periods of 4 months or less. North of this region (29–39°N) a significant spectral peak is found at a period of two years. This energy is restricted to wavelengths > 2000 km. It has been suggested (Goldenberg and O'Brien, 1981) that this 2-year peak might be associated with a shift in the southward penetration of winter storms.

The high energy in the annual peak and its increase with latitude can be attributed to the seasonal shift of the sun's position relative to the equator. Harmonics of the annual period (6, 4, 3 months, etc.) often exhibit significant energy levels because the annual signal is not a perfect sine wave. Thus, other frequencies are introduced by the annual fluctuations.

These zonal two-dimensional spectra can be divided into two zonal bands each having a unique character. Between 17 and 27°N the spectra (Figs. 3a–3f) are less coherent at the annual period, have no 2-year peak and display more energy at higher frequencies. These spectra were grouped together into a southern or tropical band (TB) while those north of 29°N (29°N–39°N) were put into the northern or subtropical band (SB).

Average frequency-wavenumber spectra, formed by averaging the spectra in each group, exhibit the properties (Figs. 4a and 4b) mentioned above. The SB shows the dominance of the annual signal at all wavenumbers. The 2-year and semiannual peaks are also significant. To the south the TB, while still dominated by the annual peak, at low wavenumbers, demonstrates more isolated energy at higher wavenumbers and frequencies. In both bands the significant spectral peaks (marked by at least two contours) are essentially symmetric with no preferred westward or eastward propagation.

### *b. Wind-stress curl*

In strong contrast to the SST spectra the frequency-wavenumber spectra of WSCL (Figs. 5a–5l) are not dominated by a peak at the annual period. South of 28°N the annual cycle does display significant energy at the lowest wavenumbers. The annual peaks are generally not symmetrical nor centered about the zero wavenumber (Figs. 5a–5c). Some (i.e., Fig. 5d) show a tendency toward eastward propagation (tongues extending toward positive wavenumbers) while others (i.e., Fig. 5a) exhibit a weak indication of westward propagation (tongues extending toward negative wavenumbers).

The spectra for these lower latitude bands also

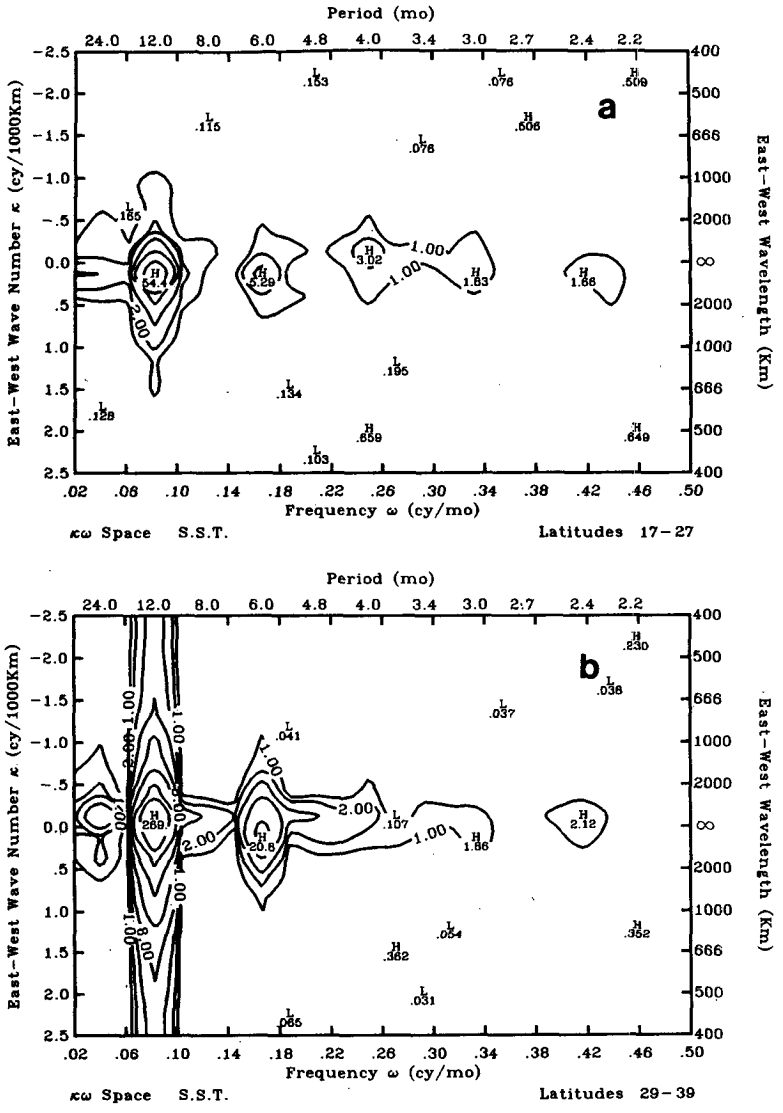


FIG. 4. Average frequency-wavenumber spectra of sea surface temperature for (a) the SB and (b) the TB.

contain many other significant peaks at higher frequencies (i.e., Figs. 5b and 5c). Most of these peaks cluster about the origin on the wavenumber axis indicating that all frequencies are primarily associated with wavelengths of basin size. This preference for energy at large wavelengths also appears in the spectra for latitudes 36 and 38°N (Figs. 5j and 5k). Here the energy levels are lower than those south of 28°N and the spectral peaks are restricted to smaller amounts of the total frequency-wavenumber space. In Fig. 5k, the northernmost spectrum contains a significant spectral peak at the annual period which is centered about 1.0 on the wavenumber axis (eastward propagation).

Between 28 and 36°N the two-dimensional WSCL spectra are essentially white. Isolated high and low energy values sprinkle the spectra with none rising above the 90% confidence interval (two contours). This complete whiteness emphasizes the stochastic nature of the smaller atmospheric disturbances in this latitude band. The region is a transition zone between the Northeast Trades to the south and the Pacific Westerlies to the north.

Even in the more coherent spectra south of 28°N there is more energy at a variety of frequencies demonstrating that shorter period fluctuations occur. That these fluctuations are predominantly of large-scale (low wavenumber) means that they represent shifts in large-scale wind systems rather than the random passage of isolated features.

The spectra in this group south of 28°N were averaged together to represent the tropical band (TB)

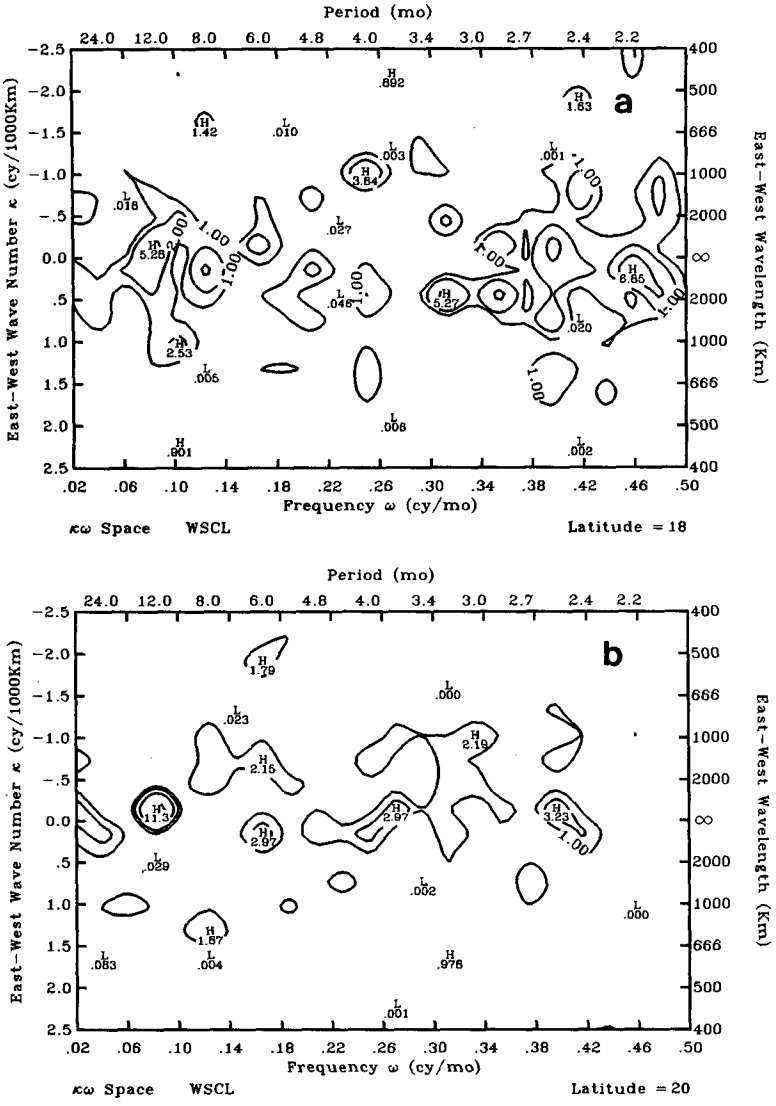


FIG. 5. Frequency-wavenumber spectra of wind-stress curl ($\log_2$ m$^2$ s$^{-4}$) for (a) 18°N, (b) 20°N, (c) 22°N, (d) 24°N, (e) 26°N, (f) 28°N, (g) 30°N, (h) 32°N, (i) 34°N, (j) 36°N and (k) 38°N.

while those north of 29°N were averaged to define the subtropical band (SB). Both average spectra are in Figs. 6a and 6b. The SB, as has been discussed, is mainly white with no significant spectral character. Note that even the low wavenumber peaks in Figs. 5j and 5k disappear when averaged in with the bands from 28 to 36°N. The TB has significant peaks at the annual, 2- and 3-month periods concentrated at the low wavenumbers.

## 5. Composite spectra

### *a. Sea surface temperature*

Reduced to frequency spectra by averaging over wavenumber, the composite frequency spectra for both the TB and the SB are presented in Fig. 7. Here the spectral energies have been converted to spectral densities as indicated by the axis label.

In the TB (solid line, Fig. 7) only the annual and semiannual peaks rise above the noise level at the given 90% confidence interval. Other than these two peaks the spectrum is relatively flat with little distinction in energy level between the lowest and highest frequencies. These regional average composite spectra appear whiter than do similar composite spectra for individual latitude bands (see the Appendix, Fig. A2).

In the SB the annual and semiannual peaks show even more energy than in the TB, and are joined as significant spectral features by the 2-year peak.

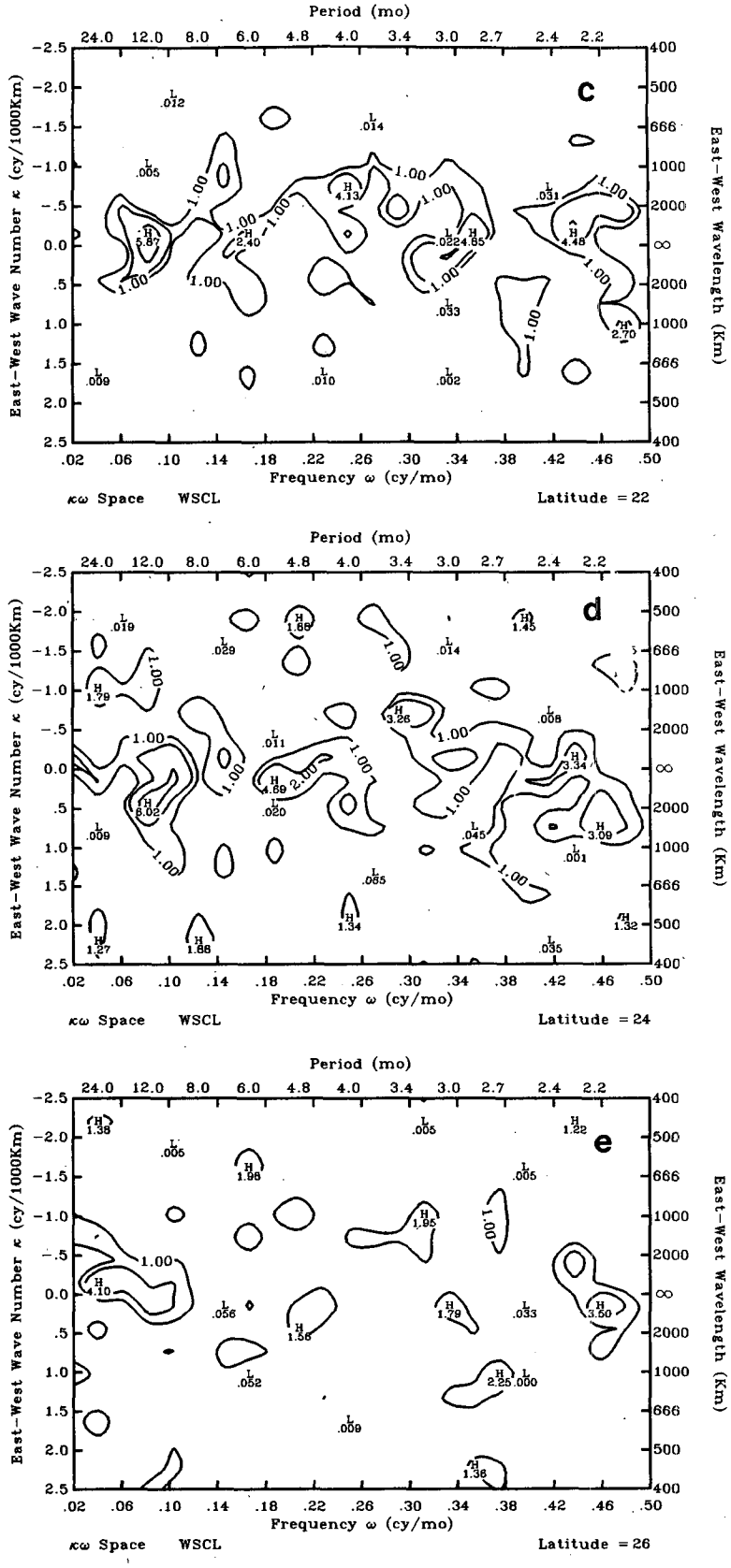


FIG. 5. (*Continued*)

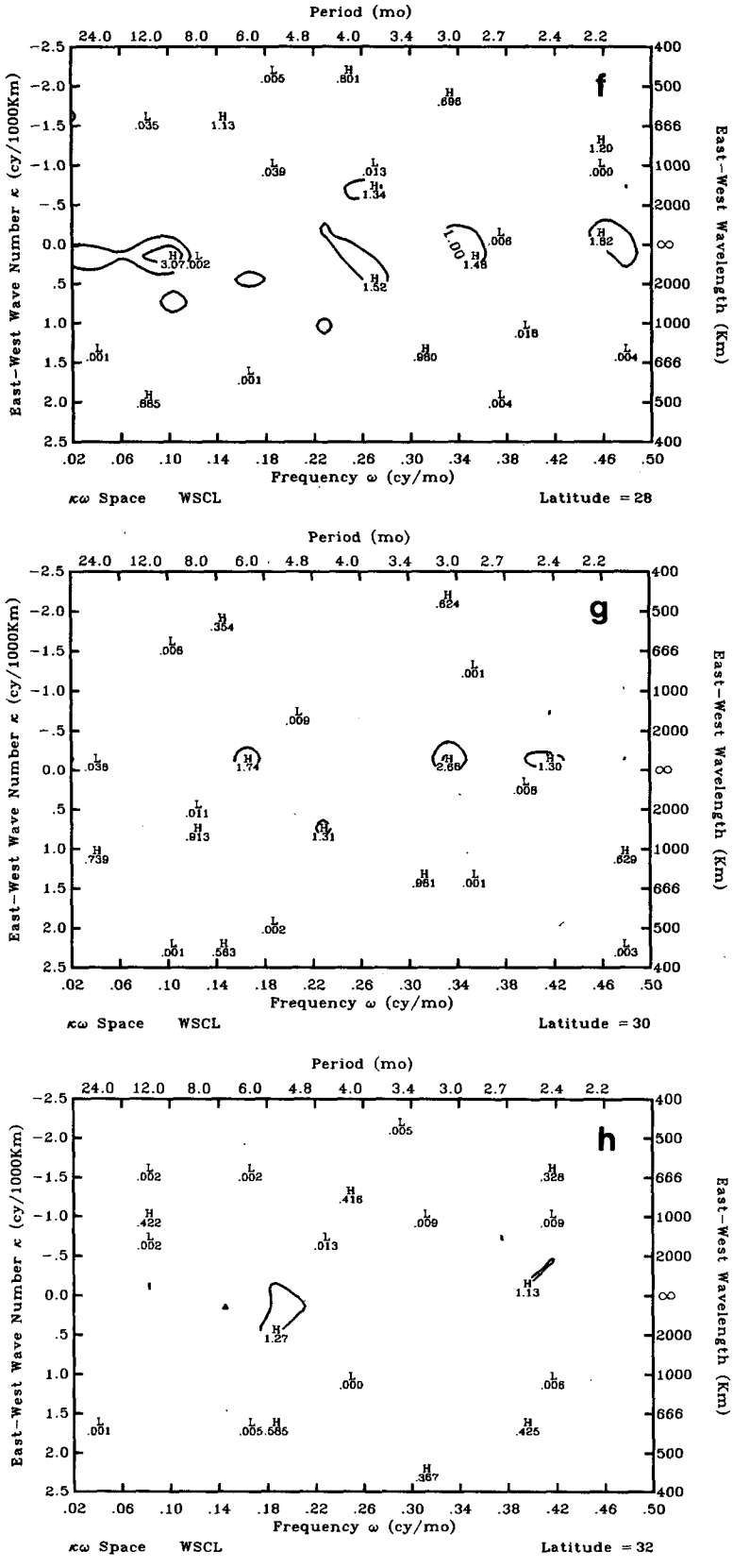


FIG. 5. (*Continued*)

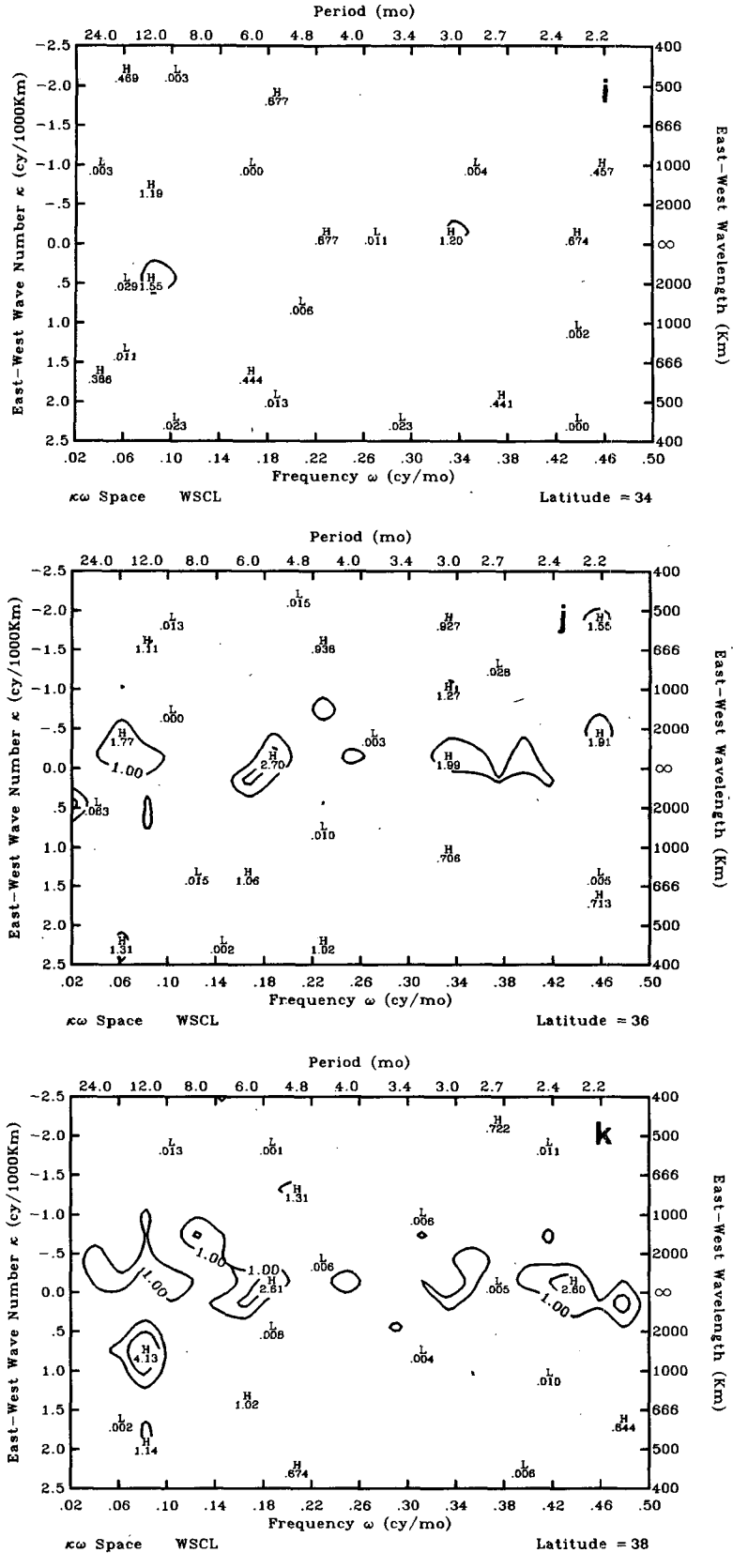


FIG. 5. (*Continued*)

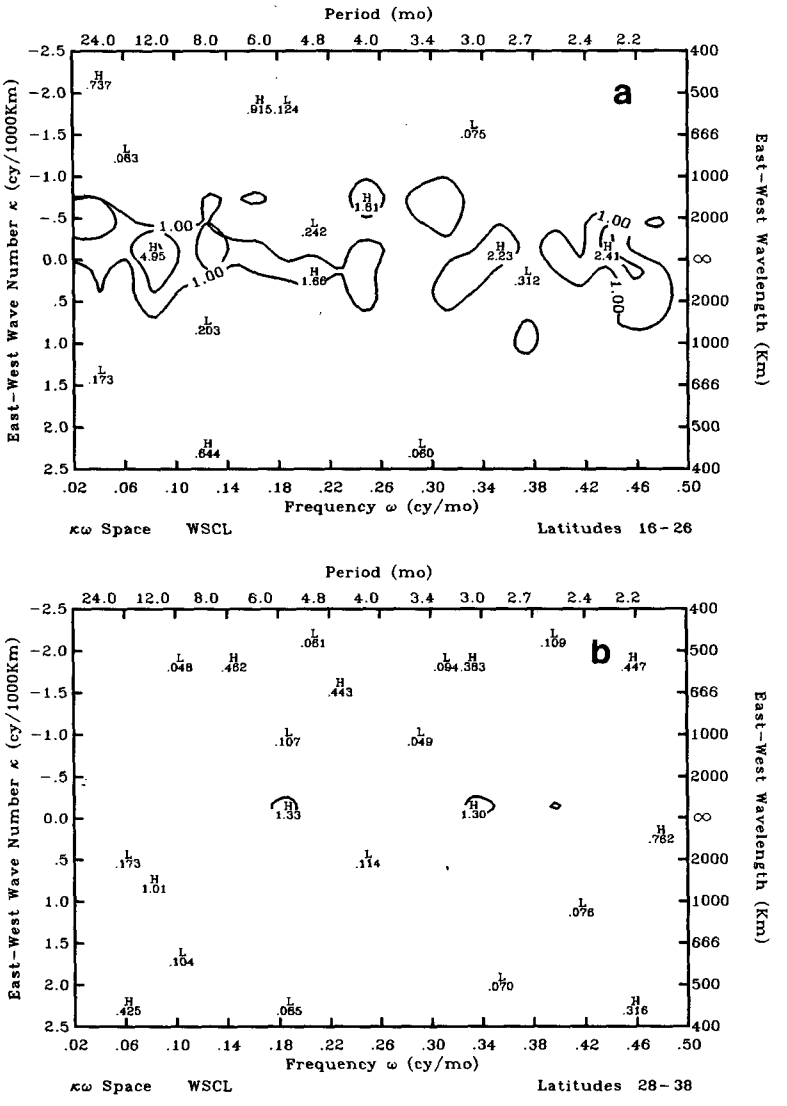


FIG. 6. Average frequency-wavenumber spectra of wind-stress curl for (a) the SB and (b) the TB.

The spectral values at periods shorter than 4 or 5 months drop somewhat below those in the TB. This shift to lower values at higher frequencies is the expression of a small negative slope with frequency in the SB. The three significant peaks (6, 12 and 48 months) contain 87% of the total SST variance in the SB, whereas the corresponding peaks in the TB explain only 42% of the variance.

Similar composite wavenumber spectra (Fig. 8) all exhibit a relatively constant fall off (red spectra) with increasing wavenumber. This almost constant negative slope is in both the east (positive) and west (negative) directions with minor asymmetries which are only slightly larger than the 90% confidence interval. This asymmetry is most apparent in the TB at the lowest wavenumbers which show a sharp discontinuity between the east and west curves. The energy levels in the TB are lower than those in the SB and the westward negative slope is smaller in the TB than in the SB. Both the SB and the TB spectra (Fig. 8) drop off with a slope of about $-1.7$ toward the east. All deviations from the nearly constant slopes, in all four curves, are not significant at the 90% level.

### *b. Wind-stress curl*

The composite frequency spectra of WSCL (Fig. 9) are essentially white for both the TB (solid line) and the SB (dashed line). Neither of these spectra exhibits any significant peaks at the 90% level. Both curves, however, have their

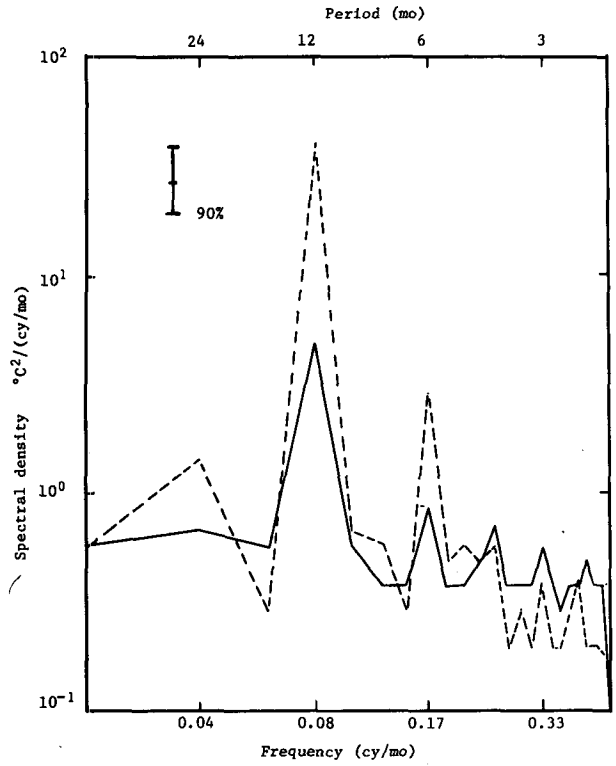


FIG. 7. Composite frequency spectra of sea surface temperature for the TB (solid line) and the SB (broken line).

maxima at the annual period with the annual peak in the TB being almost as large as the 90% confidence interval. The higher energy level in the TB spectrum, in general, is significantly (90% level) higher than that in the SB. This is in contrast to the SST composite, frequency spectra which had somewhat higher spectral energies (mainly in the 12 and 6 month peaks) in the SB (Fig. 7). The higher spectral level in the WSCL TB is an indication of the important fluctuations of WSCL associated with the Northeast Trade Winds in the eastern North Pacific (Wyrtki and Meyers, 1976).

The WSCL composite wavenumber spectra (Fig. 10) are not as red as the SST wavenumber spectra (Fig. 8). The WSCL spectra are also much more symmetric with only a very slight change in spectral level between eastward and westward components. The negative slopes in both directions are similar and are nearly constant. A small deviation from this constant slope, in the eastward direction, results in an insignificant (90% level) peak at ~1200 km in wavelength. The only feature of these spectra which is statistically significant is the higher spectral energy level in the TB over that in the SB.

## 6. Discussion of the forcing spectra

The frequency-wavenumber spectra of SST and WSCL, in the eastern North Pacific have largely confirmed the assumptions of earlier investigators. The WSCL spectra, as discussed by Willebrand *et al.* (1980), are mainly white in frequency and red in wavenumber. There is a suggestion that the annual period may contain significant energy at long wavelengths for the lower (<28°N) latitude spectra.

Stochastic generation models (Frankignoul and Hasselmann, 1977; Frankignoul and Müller, 1979a,b) necessarily neglect any deterministic forcing at particular frequencies and thus ignore the annual peak. This is perhaps more important for buoyancy flux estimates as the SST spectra are dominated by the annual, semiannual and 2-year periods. These

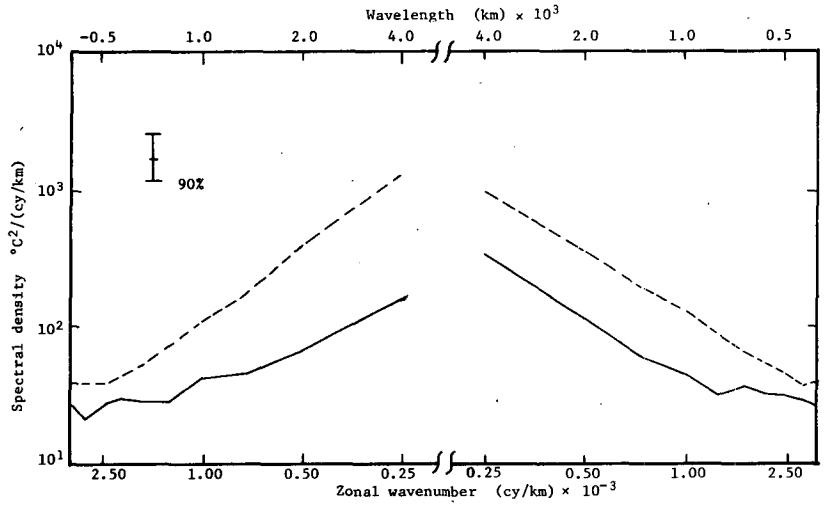


FIG. 8. Composite wavenumber spectra of sea surface temperature for the TB (solid line) and the SB (broken line).

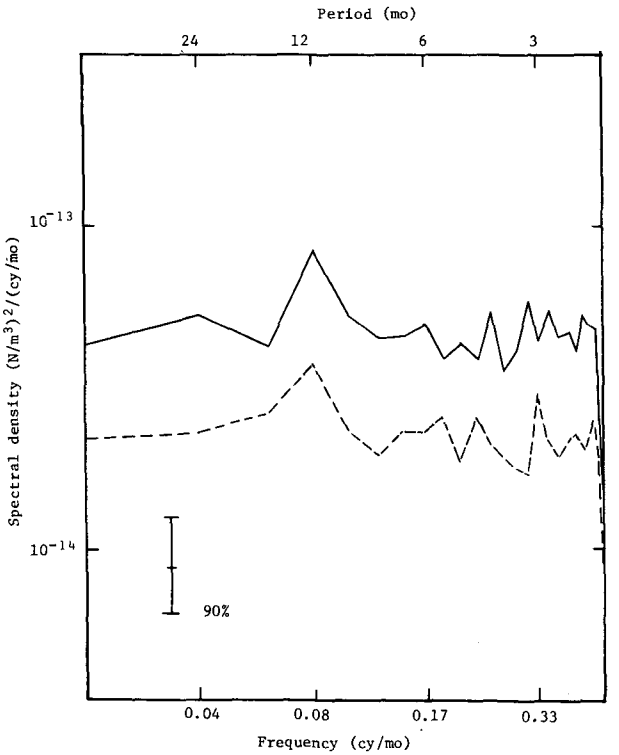


FIG. 9. Composite frequency spectra of wind-stress curl for the TB (solid line) and the SB (broken line).

stochastic studies conclude, however, that SST fluctuations are not strong enough to generate mesoscale oceanic circulations.

It is interesting to note that both SST and WSCL spectra could be naturally separated into north (SB) and south (TB) regions. The behavior of each in the respective regions is quite opposite, however, with WSCL fluctuations strongest in the southern TB and SST oscillations greatest in the SB. This relates to the strong fluctuations of WSCL at the northern edge of the Northeast Trade Winds and the role of large-scale SST anomalies at mid-latitudes (30–40°N). It suggests that perhaps different generation mechanisms are more important in some regions than in others.

The separation of all the spectra into two bands emphasizes the fact that no single forcing spectrum can be used to study the generation of oceanic motions. Regional differences in the wind field and in the processes governing SST fluctuations require the appropriate study of atmospheric data, from these regions, to estimate the input forcing spectra. Significant asymmetries in the frequency-wavenumber spectra for individual zonal bands are not well represented in even the regional averages presented in this paper. Such asymmetries may play an important role in the generation of propagating disturbances in certain limited regions.

*Acknowledgments*. The authors would like to express their appreciation to Mrs. Florace Kling for her continued support both in typing and editing. While acting as NORPAX data manager Rich Wert reduced the Marine Deck data to the form used in this study. The authors are also grateful to Carl Wunsch and Claude Frankignoul for pointing out important problems in an earlier version of this paper which led to substantial revision. This work has been supported by the U.S. Office of Naval Research, Code 480, under grants to the University of Hawaii, Texas A&M University and the Uni-

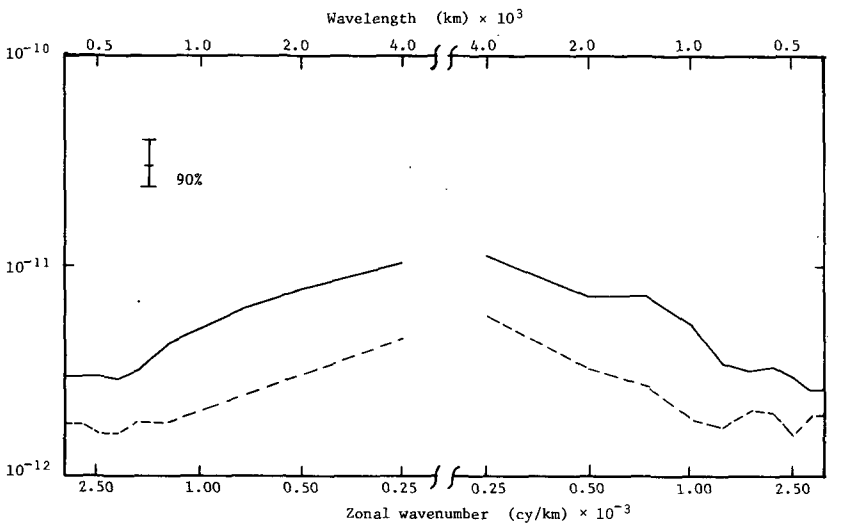


FIG. 10. Composite wavenumber spectra of wind-stress curl for the TB (solid line) and the SB (broken line).

versity of British Columbia; this support is gratefully acknowledged. This paper is Hawaii Institute of Geophysics Contribution 1135.

## APPENDIX

### Computation of the Frequency-Wavenumber Spectra

Assuming that a function of space and time can be represented by the linear superposition of a unique set of sines and cosines we can write

$$Z_{\text{obs}}(x_i, \phi_j, t_k) = \sum_l \sum_m [A_{lm}(\phi_j) \cos(\kappa_l x_i + \omega_m t_k) + B_{lm}(\phi_j) \sin(\kappa_l x_i + \omega_m t_k) + C_{lm}(\phi_j) \times \cos(\kappa_l x_i - \omega_m t_k) + D_{lm}(\phi_j) \sin(\kappa_l x_i - \omega_m t_k)],$$
$$l = 1, 2, \ldots, I/2, \quad m = 1, 2, \ldots, N/2. \quad \text{(A1)}$$

In this equation $Z_{\text{obs}}(X_i, \phi_j, t_k)$ is a subset of observations of $Z(x, \phi, t)$. Here $X$ is the distance (km) from a reference meridian, $\phi$ is latitude (deg) and $t$ is time (months).

Taking the transforms one at a time we first write the temporal transform as

$$Z_{\text{obs}}(x_i, \phi_j, t_k) = \sum_{m=1}^{N/2} [a_m(x_i, \phi_j) \cos\omega_m t_k + b_m(x_i, \phi_j) \sin\omega_m t_k]. \quad \text{(A2)}$$

Now we transform $a_m(X_i, \phi_j)$ and $b_m(X_i\phi_j)$ zonally

$$a_m(x_i, \phi_j) = \sum_l^{I/2} c_{lm}(\phi_j) \times \cos\kappa_l x_i + d_{lm}(\phi_j) \sin\kappa_l x_i, \quad \text{(A3a)}$$

$$b_m(x_i, \phi_j) = \sum_l^{I/2} e_{lm}(\phi_j) \times \cos\kappa_l x_i + f_{lm}(\phi_j) \sin\kappa_l x_i, \quad \text{(A3b)}$$

Substituting (A3a,b) back into (A2) yields

$$Z_{\text{obs}}(x_i, \phi_j, t_k) = \sum_l \sum_m \tfrac{1}{2}[c_{lm}(\phi_j) - f_{lm}(\phi_j)] \cos(\kappa_l x_i + \omega_m t_k) + \tfrac{1}{2}[d_{lm}(\phi_j) + e_{lm}(\phi_j)] \sin(\kappa_l x_i + \omega_m t_k) + \tfrac{1}{2}[c_{lm}(\phi_j) + f_{lm}(\phi_j)] \cos(\kappa_l x_i - \omega_m t_k) + \tfrac{1}{2}[d_{lm}(\phi_j) - e_{lm}(\phi_j)] \sin(\kappa_l x_i - \omega_m t_k), \quad \text{(A4)}$$

which is equivalent to (1) if

$$\left.\begin{aligned} A_{lm}(\phi_j) &= \tfrac{1}{2}[c_{lm}(\phi_j) - f_{lm}(\phi_j)] \\ B_{lm}(\phi_j) &= \tfrac{1}{2}[d_{lm}(\phi_j) + e_{lm}(\phi_j)] \\ C_{lm}(\phi_j) &= \tfrac{1}{2}[c_{lm}(\phi_j) + f_{lm}(\phi_j)] \\ D_{lm}(\phi_j) &= \tfrac{1}{2}[d_{lm}(\phi_j) - e_{lm}(\phi_j)] \end{aligned}\right\}. \quad \text{(A5)}$$

Thus the frequency-wavenumber spectrum of $Z_{\text{obs}}(X_i, \phi_j, t_k)$ is

$$E_z(\kappa_l, \omega_m, \phi_j) = C_{lm}^2(\phi_j) + D_{lm}^2(\phi_j), \quad \text{(A6a)}$$

$$E_z(\kappa_{-l}, \omega_m k\phi_j) = A_{lm}^2(\phi_j) + B_{lm}^2(\phi_j), \quad \text{(A6b)}$$

where $+l$ corresponds to eastward propagation [Eq. (A6a) and $-l$ corresponds to westward propagation [Eq. (A6b)].

This procedure would have been followed exactly if there had been no gaps in the time series. Missing months, however, motivated the use of a least-squares method in calculating the temporal transform of Eq. (A2). In this method the coefficients $a_m$ and $b_m$ are found by solving the normal equations

$$\frac{\partial}{\partial a_m} \sum_{k=1}^{\text{number of observations}} \{Z_{\text{obs}}(x_i, \phi_j, t_k) - \sum_{m=1}^{M} [a_m(x_i, \phi_j) \cos\omega_m t_k + b_m(x_i, \phi_j) \sin\omega_m t_k]\}^2 = 0, \quad \text{(A7a)}$$

$$\frac{\partial}{\partial b_m} \sum_{k=1}^{\text{number of observations}} \{Z_{\text{obs}}(x_i, \phi_j, t_k) - \sum_{m=1}^{M} [a_m(x_i, \phi_j) \cos\omega_m t_k + b_m(x_i, \phi_j) \sin\omega_m t_k]\}^2 = 0. \quad \text{(A7b)}$$

In order to evaluate the reliability of this computational technique, frequency spectra were com-

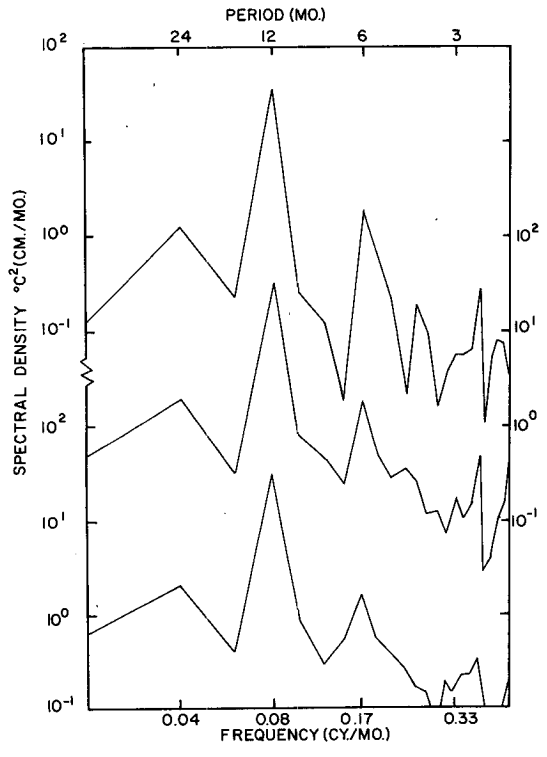


FIG. A1. Frequency spectra of a uniformly sample time series as calculated according to the least-squares method (upper plot), Bartlett method (middle line) and standard Fourier method (lower line).

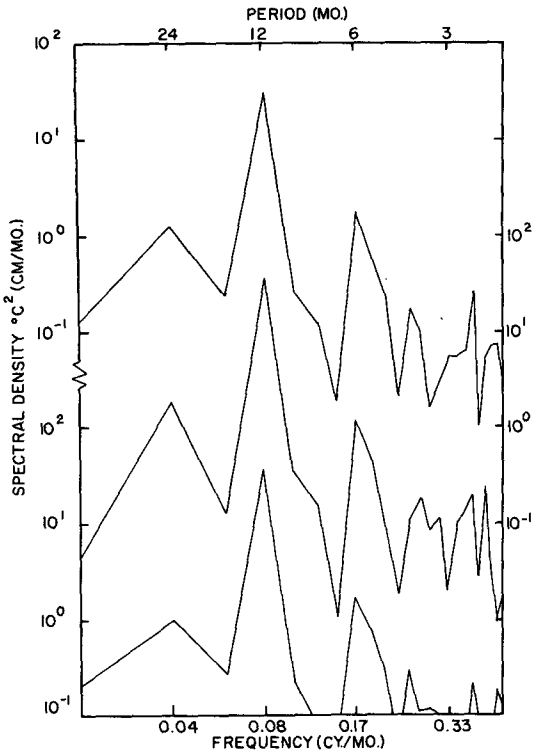


FIG. A2. Frequency spectra of a time series as calculated according to the least-squares method (LSQ) when the time series has no missing observations (upper plot), 14 missing observations (lower plot), and 15 missing observations (middle plot).

puted from an SST time series using this method (LSQ) and two familiar spectral methods. The first was a standard Fourier technique and the second (called Bartlett's procedure) partitions the time series into subsets before transforming. The input series used to compute the spectra in Fig. A1 was continuous with no temporal gaps. For presentation the $\log_{10} - \log_{10}$ spectra are separated by two decades.

It is apparent that the basic spectral shape is well represented by the LSQ method. The strong spectral peaks, especially at the lower frequencies, show up in all three methods. The generally lower spectral level of the LSQ method reveals that it underestimates the series variance. This method also produces a slightly larger 6-month peak than do the other methods. A peak at about 4.5 months in the LSQ spectrum does not show up in the other two spectra.

Using only the LSQ method some missing data were introduced at random to the series. In Fig. A2 LSQ spectra are presented for the same SST series without gaps, with 14 missing points and with 15 missing points. These spectra demonstrate that most of the changes, due to the missing data (gaps), occur at the higher frequencies. The stronger low-frequency peaks are only slightly altered in either shape or magnitude. Thus for strong deterministic signals like those in the SST series the LSQ method compares well with both the standard Fourier and Bartlett's techniques.

To estimate the degrees of freedom in each LSQ spectral estimate it was reasoned that the number of degrees of freedom should be the same as that for a continuous record and a standard transform method. Using an 11-year record and a fundamental period of four years each spectral estimate in a frequency spectrum would have about six degrees of freedom. Thus for the two-dimensional frequency-wavenumber spectra a total of 12 degrees of freedom was assigned to each spectral estimate.

Further details of this method are given by Gallegos-Garcia (1980).

## REFERENCES

Emery, W., and L. Magaard, 1976: Baroclinic Rossby waves as inferred from temperature fluctuations in the eastern Pacific. *J. Math. Res.*, **34**, 365–385.

Frankignoul, C., and K. Hasselmann, 1977: Stochastic climate models, part II. Application to sea-surface temperature anomalies and thermodine variability. *Tellus*, **29**, 289–305.

——, and P. Müller, 1979a: Quasi-geostrophic response of an infinite $\beta$-plane ocean to stochastic forcing by the atmosphere. *J. Phys. Oceanogr.*, **9**, 104–127.

——, and ——, 1979b: On the generation of geostrophic eddies by surface buoyancy flux anomalies. *J. Phys. Oceanogr.*, **9**, 1207–1213.

Gallegos-Garcia, A., 1980: Frequency-wavenumbers spectra of sea surface temperature and wind stress in the eastern North Pacific and their relation to locally forced low-frequency fluctuations in the ocean. Ph.D. dissertation, Texas A & M University, 150 pp.

Goldenberg, S. B., and J. J. O'Brien, 1981: Time and space variability of tropical Pacific wind stress. *Mon. Wea. Rev.*, **109**, 1190–1207.

Kao, S. K., 1970: Wavenumber-frequency spectra of temperature in free atmosphere. *J. Atmos. Sci.*, **27**, 1000–1007.

Kenyon, K. E., 1977: A large-scale longitudinal variation in surface temperature in the North Pacific. *J. Phys. Oceanogr.*, **7**, 256–263.

Magaard, L., 1977: On the generation of baroclinic Rossby waves in the ocean by meteorological forces. *J. Phys. Oceanogr.*, **7**, 359–364.

Saunders, P. M., 1976: On the uncertainty of wind stress curl calculations. *J. Mar. Res.*, **34**, 155–160.

Saur, J. F. T., 1963: A study of the quality of seawater temperature reported in logs of ship's weather observations. *J. Appl. Meteor.*, **2**, 417–425.

Tabata, S., 1978: An evaluation of the quality of sea surface temperatures and salinities measured at station P and line P in the northeast Pacific Ocean. *J. Phys. Oceanogr.*, **8**, 970–986.

Wallace, J. M., and C. P. Chang, 1969: Spectrum analysis of large-scale disturbance in the tropical lower troposphere. *J. Atmos. Sci.*, **26**, 1010–1025.

Willebrand, J., 1978: Temporal and spatial scales of the wind field over the North Pacific and North Atlantic. *J. Phys. Oceanogr.*, **8**, 1080–1094.

——, S. G. H. Philander and R. C. Pacanowski, 1980: The oceanic response to large-scale atmospheric disturbances. *J. Phys. Oceanogr.*, **10**, 411–429.

Wilson, M. A. G., 1975: A wavenumber-frequency analysis of large-scale tropospheric motions in the extratropical Northern Hemisphere. *J. Atmos. Sci.*, **32**, 478–488.

Wyrtki, K., and G. Meyers, 1976: The tradewind field over the Pacific Ocean. *J. Appl. Meteor.*, **15**, 698–704.